Real-Time Process Monitoring of Micromolding Using Integrated Ultrasonic Sensors

Ono, Y.; Whiteside, B. R.; Brown, E. C.; Kobayashi, Makiko; Cheng, C. -C.; Jen, Cheng-Kuei; Coates, P. D.

Publisher's version / Version de l'éditeur:
https://doi.org/10.1177/0142331207080153
Transactions of the Institute of Measurement and Control, 29, December 5, pp. 383-401, 2007-10-01

Real-Time Process Monitoring of Micromolding using Integrated Ultrasonic Sensors

Y. Ono[1], B.R. Whiteside[2], E.C. Brown[2], M. Kobayashi[1], C.-C. Cheng[3,4], C.-K. Jen[1], and, P.D. Coates[2]

[1] Industrial Materials Institute, National Research Council Canada, Boucherville, Quebec, Canada, J4B 6Y4

[2] IRC in Polymer Science & Technology, University of Bradford, Bradford, UK, BD7 1DP

[3] Dept. of Electrical and Computer Engineering, McGill University, Montreal, Quebec, Canada, H3A 2A4

[4] Permanent address: Dept. of Electrical Engineering, Hsiuping Institute of Technology, Da-Li, Taichung, Taiwan

Correspondence:

Yuu ONO, Ph.D.

Research Officer

Industrial Materials Institute, National Research Council Canada

75 Boul. de Mortagne, Boucherville, Quebec, Canada, J4B 6Y4

Tel: (1) 450-641-5086/Fax (1) 450-641-5106

Email: yuu.ono@cnrc-nrc.gc.ca

Abstract

Real-time, non-intrusive and non-destructive process monitoring of micromolding has been performed using novel ultrasonic sensors integrated onto the barrel and mold insert with ultrasonic pulse-echo technique. The relative variation of the polymer melt temperature inside the barrel can be obtained using the ultrasonic velocities of the melt measured at the barrel during extrusion. Melt flow arrival, solidification and shrinkage of the polymer inside the mold cavity were also successfully monitored. The presented ultrasonic sensors and technique enable optimizing the micromolding process, and improving quality of the molded parts and process efficiency.

Key words: Process monitoring; micromolding; high temperature ultrasonic transducer; solidification; shrinkage; detachment.

Nomenclature

L^n	n-th round trip ultrasonic longitudinal-wave echo propagating in the barrel or mold insert
L_{2n}	n-th round trip ultrasonic longitudinal-wave echo propagation in the polymer inside the barrel or mold cavity
v_b	Ultrasonic velocity of the polymer inside the barrel
h_b	Distance between the internal surface of the barrel and screw root
Δt_b	Time delay difference of the echo reflected from the internal surface of the barrel and that from the screw root
v_m	Ultrasonic velocity of the polymer inside the mold cavity
h_m	Depth of the mold cavity

Δt_m Time delay difference of the echo reflected from the mold cavity surface and that from the immobile mold surface

T_c Crystallization temperature

v_c Crystallization ultrasonic velocity

T_s Solidus temperature

v_s Solidus ultrasonic velocity

Subscript

n The number of round trip

b Barrel

m Mold

c Crystallization

s Solidus

Acronyms

HT High temperature

UT Ultrasonic transducer

SNR Signal-to-noise ratio

BIT Bismuth titanate

PZT Lead-zirconate-titanate

POM Polyoxymethylene

1. Introduction

Micromolding technology has realized the mass production of MEMS components at a fraction of the cost of lithographic and silicon etching techniques (Benzler, 1999; Tom, 2002). In this technology, accurate process monitoring is required to ensure process stability but integration of sensors into small and highly detailed mold units can be problematic. Therefore, in addition to conventional temperature and pressures sensors, new sensors and technique capable of monitoring physical and rheological properties of materials during extruding and molding is highly desired. Ultrasonic method is chosen in this study because of its ability to probe the properties of polymers within the steel barrel and mold during polymer processing (Piché, 1995; Brown, 1999; Wen, 1999; França, 2000; Kiehl, 2001; Edwards, 2001).

Recently we have successfully developed high temperature (HT) piezoelectric film ultrasonic transducers (UTs) (Kobayashi, 2004). Unique features of such HTUTs are as follows: they (1) are applicable at temperatures higher than 400°C; (2) can be fabricated on flat and curved surfaces; (3) can be miniaturized and integrated; (4) do not need ultrasonic couplant; (5) can be operated in low and medium MHz frequency range with sufficient frequency band width; and (6) have sufficient piezoelectric strength and signal-to-noise ratio (SNR).

It is our intention to monitor the entire micromolding process from the feed hopper to the part exit. Thus, these HTUTs were fabricated onto the barrel and mold insert of a micromolding machine, Microsystem50 from Battenfeld, Austria. The sensor fabrication technique and ultrasonic measurement data obtained by ultrasonic pulse echo technique during micromolding will be presented. Real-time, non-intrusive and non-destructive monitoring of melt temperature at the barrel, melt arrival in the mold, and solidification and shrinkage of the polymer inside the mold cavity will be demonstrated.

2. Ultrasonic Sensors

2.1 At barrel

Fine Bismuth titanate (BIT) powders were dispersed in lead-zirconate-titanate (PZT) solution and coated on the external surface of the steel barrel by an air spray gun (Kobayashi, 2004). Then drying, firing, annealing and poling processes were conducted to achieve piezoelectricity of the film. Such BIT/PZT film UTs can operate at temperature up to 400°C, which is high enough for almost all polymer materials to be melted at the barrel of micromolding. Fig. 1 shows seven UTs (UT1-7) fabricated directly onto the external surface of the barrel. The diameter of the top electrode was 5mm, which is the active area size of the UT. The barrel itself served as a bottom electrode. The length of the barrel was 265mm, the internal diameter was 14mm, and the external diameter at the areas of UT1-3, 5-7 and at that of UT4 were 40mm and 30mm, respectively.

A schematic view of a cross-section of the barrel with the UT and the extrusion screw is presented in Fig. 2, explaining the paths of ultrasound propagating in the barrel and polymer melt. L^n (n=1,2,3,..) denotes n-th round trip longitudinal-wave ultrasonic echo reflected from the internal surface of the barrel, and L_2 is the first echo propagating in the melt and reflected from the screw root. Fig. 3(a) shows a typical result of longitudinal-wave ultrasonic signals reflected from the internal surface of the barrel at 240°C, measured with the UT6 in Fig. 1. The SNR of the L^1 echo was 30dB. Fig. 3(b) shows frequency spectrum of the L^1 echo in Fig. 3(a). The center frequency of the L^1 echo was 8.6MHz and 6dB bandwidth was 4.4MHz. The performance of UT1-7 was almost the same.

2.2 At mold insert

Fig. 4(a) shows a photograph of a steel mold insert having a mold cavity. The dimensions of the mold insert were 75mm in diameter and 7.5mm in thickness, respectively, and those of the cavity were 20mm-long, 2mm-wide and 0.5mm-deep. Two PZT/PZT film UTs (UT1 and UT2) were fabricated on the opposite side of the cavity with an interval of 16mm and with the diameter of the top electrode of 4mm, as shown in Fig. 4(b). The UTs were located above the both edges of the cavity as illustrated in Fig. 5. In Fig. 5, L^n (n=1,2,...) represents n-th round trip echoes reflected from the cavity surface of the mold insert, and L_{2n} is those propagating in the polymer and reflected at the polymer/immobile mold interface.

Fig. 6(a) and (b) show longitudinal-wave ultrasonic signals reflected from the cavity surface of the mold insert and the frequency spectrum of the L^1 echo at 100°C, measured with the UT1 in Fig. 4(b). The SNR of the L^1 echo was 30dB. The center frequency of the UTs was 9MHz and 6dB bandwidth was 7MHz. It is noted that the PZT/PZT UTs, fabricated at the mold insert, have 10dB stronger ultrasonic signals but lower operation temperature up to 250°C, which is high enough at the mold for micromolding, than the BIT/PZT UTs at the barrel.

3. Experimental Setup

After the fabrication of the UTs, the barrel and mold insert were assembled to the micromolding machine. An ultrasonic data acquisition system was composed of Panametrics 5072 pulser-receivers, Gage Applied Science 12100 dual-channel digitizing board having a resolution of 12-bit and a sampling rate of 50MHz for each channel, and a personal computer with data acquisition and analysis programs by LabVIEW. The signals were acquired every 1ms at the mold insert and every 50ms at the barrel during the whole molding cycle (8s) in the pulse-echo mode. In addition, the micromolding machine was equipped with Dynisco PCI-4011 and PCI-4006 piezo load transducers for injection and cavity pressure measurements, respectively,

Temposonics R-series displacement transducer for displacement and velocity measurements of the injection pin, and J-type thermocouples for mold temperature measurements (Whiteside, 2003).

The material employed was a polyacetal copolymer (polyoxymethylene: POM, grade: POM109C) from Chem Polymer, UK. A typical molding condition employed in the experiments was as follows: melt and mold temperatures were 200°C and 75°C, respectively; injection pin speed was 500mm/s; and holding and cooling time was 0.3s and 5s, respectively. A photograph of a molded part is given in Fig. 7. The sprue and runner area of the part was removed and not shown in the photograph. The white dotted circles indicate the positions of the UT1 and UT2 on the mold insert in Fig. 4(b) and Fig. 5.

4. Experiments and Results

4.1 At barrel

Fig. 8 shows a typical waveform acquired with the UT6 at the barrel in Fig. 1. One can see the L_2 echo reflected at the polymer melt/screw root interface, as illustrated in Fig. 2. The width of the screw root was 5mm, which is comparable to the UT size (5mm) at the barrel. The gap distance between the internal surface of the barrel and the screw root was 3.275mm. The signals reflected from the root had the SNR of more than 10dB and enable the measurement of ultrasonic velocity and attenuation in the polymer melt.

Ultrasonic propagation characteristics (velocity and attenuation) in the polymer are strongly related to the material properties (viscosity, density, composition, etc.) and process parameters (temperature and pressure) (Piche, 1988). Thus, such characteristics can be used to monitor the polymer state during polymer processing. The ultrasonic velocity, v_b, in polymer melt inside the barrel can be determined by $v_b = 2h_b/\Delta t_b$, where h_b is the gap distance between the

internal surface of the barrel and the screw root at the UT location in Fig. 2, and Δt_b is the time delay difference between the L^1 and L_2 in Fig. 8. In addition, the attenuation can be determined using the amplitude difference between the L_2 and L_4, where the L_4 is the second round trip echo propagating in the polymer (the echo is not shown in Fig. 8).

Fig. 9 shows the variation of the ultrasonic velocity measured with the UT6 at the barrel with different barrel temperatures of 180, 200 and 220°C, and screw rotation speeds of 15 (squares), 30 (circles) and 45rpm (triangles). The velocities linearly decreased with respect to the barrel temperature in this temperature range. From such information, we can determine the variation of the average temperature of the melt in the barrel using the ultrasonic velocity measured. The detailed explanation will be given in Discussion.

4.2 At mold insert

Fig. 10 presents the trace of waveforms acquired with the UT1 at the mold insert in Fig. 4(b) with respect to the process time during one cycle of molding. Only a portion of the acquired signals from 0.4s to 1.0s with a process time interval of 5ms are shown in the figure though the signals were acquired every 1ms for the entire one cycle (8s) as mentioned previously. One can see the L^1 and L^2 echoes reflected from the mold cavity surface of the mold insert. After the polymer melt arrived at the UT location, the L_2, L_4 and L_6 echoes were observed while the polymer contacted the cavity surface. The ultrasonic velocity, v_m, in polymer melt inside the mold cavity can be determined by $v_m = 2h_m/\Delta t_m$, where h_m is the depth of the cavity at the UT location in Fig. 5, and Δt_m is the time delay difference between the L_2 and L_4 in Fig. 10. The ultrasonic velocities measured at the mold insert during molding will be presented in section 4.4.

4.3 Relationship between ultrasonic signals and molding cycle

In order to investigate further the correlation between the ultrasonic signals observed and the molding cycle, the amplitude values of the L^1 and L_2 echoes with respect to the process time were obtained using the signals measured with the UT1 at the mold insert. The results are presented in Fig. 11. At process time of 0.45s, the polymer melt arrived at the cavity area beneath the UT1, since the amplitude of the L^1 echo decreased and the L_2 echo started to appear as seen in Fig. 11 due to the fact that a part of the ultrasonic energy was transmitted into the polymer through the mold insert/polymer interface and then reflected back at the polymer/immobile mold interface as shown in Fig. 5. At 0.96s, the amplitude of the L^1 echo recovered to the almost initial value and the L_2 echo disappeared, because of total reflection at the polymer/air interface, indicating that the molded part was detached from the surface of the mold cavity. This will be further discussed later. At 6s, slight increase of the amplitude of the L^1 echo was observed when the mold opened.

4.4 Solidification and shrinkage

Here, we use the ultrasonic velocity to investigate the polymer state in the cavity during molding. Fig. 12 presents the ultrasonic velocities with respect to the process time obtained with the UT1, together with the amplitude variation of the L^1 echo in Fig. 11. At 0.45s, the polymer melt arrived at the UT1 area as mentioned previously, and the ultrasonic velocity of the polymer measured was 1240m/s. Then the velocity gradually increased up to 1500m/s, suggesting the solidification of the polymer melt due to cooling by the lower mold temperature (75°C) than the melt.

The amplitude of the L^1 in Fig. 12 increased gradually after 0.86s, indicating the part was partially detached from the mold cavity surface due to the shrinkage of the part solidified. During the melt solidifying, the shrinkage of the polymer was compensated with the additional

melt by the holding pressure, and the contact between the polymer and the cavity surface was kept steadily. However, once the melt was completely solidified, the polymer is no longer added into the cavity because of the frozen of the gate.

During the part shrinkage from 0.86s to 0.96s, the decrease of the velocity was observed in Fig. 12, which will be further discussed later. At 0.96s, the part detached from the mold cavity as described previously. Thus, further cooling may not have been necessary after 0.96sec, and a reduction of the cooling time may be practiced. From this information, we can reduce the cycle time so as to improve the process efficiency of part manufacturing.

5. Discussion

In order to predict the state of the polymer inside the cavity during molding using the ultrasonic velocities in Fig. 12, we have conducted an off-line measurement of ultrasonic properties of the same POM using a static ultrasonic measurement system (Piche, 1988). This system can measure the specific volume, ultrasonic velocity and ultrasonic attenuation of the polymeric materials simultaneously with a function of temperature and pressure. Details of this system can be found in (Piche, 1988). The measurement was conducted in the temperature range from 210°C to 50°C during cooling with a constant pressure of 10MPa. Ultrasonic frequency of an UT employed was 2.5MHz and the cooling rate was –2°C/min.

The measured ultrasonic velocity and attenuation of the POM are given in Fig. 13(a). During cooling, the ultrasonic velocity and attenuation started to increase steeply at 157°C, corresponding to crystallization temperature, T_c (Tatibouet, 1991). At T_c, crystallization ultrasonic velocity, v_c, was 1253m/s. Such steep increase in velocity and attenuation continued until the temperature reached to 150°C, which is solidus temperature T_s. From 157°C to 150°C, sharp increase of the velocity and attenuation was caused by the crystallization of the POM, in

which phase transformation of the POM from liquid to solid state occurred. At 150°C, the solidus velocity, v_s, was obtained to be 1447m/s. From 157°C to 150°C, the specific volume of the POM, presented in Fig. 13(b), also showed sharp reduction. Therefore, the polymer state inside the mold cavity during molding can be predicted using the velocities measured as follows: the polymer is in the liquid state when the velocity is lower than v_c (1253m/s); and in the solid state if higher than v_s (1447m/s), in the temperature range from 210°C to 50°C at 10MPa.

In the liquid state, the velocity changing ratio with the melt temperature was –1.78(m/s)/°C in the range between 180°C and 210°C in Fig. 13(a), which is almost the same as that with the barrel temperature, –1.76±0.11(m/s)/°C, obtained from the three data with different rotation speeds in Fig. 9. Thus, the relative variation of the temperature of the melt in the barrel can be obtained using the ultrasonic velocities measured at the barrel during extrusion as mentioned previously.

Here our intension is to interpret the solidification behavior of the POM in the mold insert by correlating the off-line measurement results in Fig. 13 to the ultrasonic velocities in Fig. 12 obtained during molding. It is noted that temperature dependence of the material properties in Fig. 13 is sensitive to the thermal history of the material, pressure and ultrasonic frequency employed. Therefore, we can only explain the behavior of the POM in the mold cavity qualitatively since the cooling rate in the molding was much larger than that in the off-line measurements. In the molding, the melt (200°C) was cooled down to mold temperature (75°C) within 8s under the presented molding condition while in the off-line measurements the cooling rate was –2°C/min as mentioned previously. In addition, the cavity pressure during molding was not constant (Whiteside, 2003).

When the polymer melt was injected into the mold cavity, the velocity was about 1240m/s at 0.45s, as shown in Fig. 12, which was just slightly smaller than v_c, indicating that the

polymer was in the liquid state. Then the velocity increased gradually and reached to constant and maximum value of 1500m/s at 0.72sec in Fig. 12, which is larger than v_s, indicating that polymer was in the solid state. During the shrinkage from 0.86s to 0.96s, the decrease of the velocity was observed in Fig. 12. It is believed that a thin air layer partially developed between the cavity surface and the polymer caused the decrease of the velocities measured.

6. Conclusion

Real-time, non-intrusive and non-destructive process monitoring of micromolding has been performed using novel integrated high temperature ultrasonic sensors developed. The ultrasonic sensors were fabricated directly onto the barrel and mold insert of a micromolding machine by a sol-gel spray technique. Ultrasonic monitoring of micromolding for 20mm-long, 2mm-wide and 0.5mm-thick parts was demonstrated with a polyacetal copolymer. Clear ultrasonic signals have been obtained at the barrel and mold insert during molding in ultrasonic pulse-echo technique.

The relative variation of the temperature of the melt in the barrel can be obtained using the ultrasonic velocity measured at the barrel during extrusion. Flow arrival of the polymer melt inside the mold cavity and part detachment from the cavity due to the shrinkage was probed using the amplitude variation of the echo reflected from the cavity surface of the mold insert. Such information can be used to control the injection pin speed and cooling time, enabling improvement of the process efficiency of part manufacturing by reducing the cycle time.

The solidification monitoring of the molded part in the cavity was performed by measuring the ultrasonic velocity in the part using the multiple echoes propagating in the part. The variation of ultrasonic velocity reflects the material properties of the part, such as elastic constants, viscosity and density, during the solidification. Thus, it is demonstrated that presented

ultrasonic sensors and technique enable optimizing the micromolding process, and improve the part quality and process efficiency by reducing cycle time.

Acknowledgments

The authors acknowledge to financial supports of the Joint Science and Technology Fund of National Research Council of Canada and British Council for the Researcher Exchange Awards, and the Natural Sciences and Engineering Research Council of Canada.

References

- **Benzler, T., Piotter, V., Hanemann, T., Mueller, K., Norajitra, P., Ruprecht, R.** and **Hausselt, J.** 1999: Innovations in molding technologies for microfabrication. *Proc. of SPIE* 3874, 53-60.
- **Brown, E.C., Collins, T.L.D., Dawson, A.J., Olley, P.** and **Coates P.D.** 1999: Ultrasound: a virtual instrument approach for monitoring of polymer melt variables. *J. Reinf. Plast. Comp.*, 18, 331-338.
- **Edwards, R. and Thomas, C.** 2001: On-line measurement of polymer orientation using ultrasonic technology. *Polymer Engineering and Science* 41, 1644-1653.
- **França, D.R., Jen, C.-K., Nguyen, K.T.** and **Gendron, R.** 2000: On-line ultrasonic monitoring of polymer extrusion. *Polymer Engineering and Science* 40, 82-94.
- **Kiehl, C., Chu, L.-L., Letz, K.** and **Min, K.** 2001: On-line ultrasonic measurements of methyl methacrylate polymerization for application to reactive extrusion. *Polymer Engineering and Science* 41, 1078-1086.

- **Kobayashi, M.** and **Jen, C.-K.** 2004: Piezoelectric thick bismuth titanate/lead zirconate titanate composite film transducers for smart NDE of metals. *Smart Materials and Structures* 13, 951-956.
- **Piche, L., Massines, F., Hamel, A.** and **Neron, C.** 1988: Ultrasonic characterization of polymers under simulated conditions. U.S. Patent 4,754,645.
- **Piché, L., Hamel, A., Gendron, R., Dumoulin, M.** and **Tatibouët, J.** 1995: Ultrasonic characterization of polymer melts under processing conditions. US Patent 5,433,112.
- **Tatibouet, J.** and **Piché, L.** 1991: Ultrasonic investigation of semicrystalline polymers: study of poly(ethylene terephthalate), *Polymer* 32, 3147-3153.
- **Tom, A.M.** and **Coulter, J.P.** 2002: Advancements in micro-molding for small-scale product fabrication. *Proc. of ASME International Mechanical Engineering Congress & Exposition*, 1-9.
- **Wen, S.-S. L., Jen, C.-K.** and **Nguyen, K.T.** 1999: Advances in on-line ultrasonic monitoring of the injection molding process using ultrasonic techniques. *Int'l Polymer Processing* XIV, 175-182.
- **Whiteside, B.R., Martyn, M.T., Coates, P.D., Allan, P.S., Hornsby, P.R.** and **Greenway, G.** 2003: Micromoulding: process characteristics and product properties. *Plastics, Rubber and Composites* 32, 231-239.

Figure captions

Fig. 1: Photograph of the barrel with seven BIT/PZT film UTs (UT1-7).

Fig. 2: Schematic view of cross-section of the barrel with the UT and the extrusion screw, showing the paths of ultrasonic signals propagating in the barrel and polymer melt.

Fig. 3: Longitudinal-wave ultrasonic signals reflected from the internal surface of the barrel (a); and frequency spectrum of the L^1 echo (b) at 240°C, measured with the UT6 in Fig. 1.

Fig. 4: Photographs of the mold insert having a cavity with dimensions of 20mm-long, 2mm-wide and 0.5mm-deep (a); and two PZT/PZT film UTs (UT1 and UT2) fabricated on opposite side of the cavity (b).

Fig. 5: Cross-sectional view of the mold insert with the UTs and the paths of ultrasonic signals propagating in the mold insert and polymer melt.

Fig. 6: Longitudinal-wave ultrasonic signals reflected from the cavity surface of the mold insert (a); and frequency spectrum of the L^1 echo (b) at 100°C, measured with the UT1 in Fig. 4(b).

Fig. 7: Photograph of a molded part. The white dotted line circles indicate the location of the UTs above the cavity in Fig. 4 and Fig. 5. The sprue and runner area of the part was removed and not shown in the photograph.

Fig. 8: Typical signals measured with the UT6 at the barrel in Fig. 1. L_2 is the echo reflected at the polymer/screw root interface, as illustrated in Fig. 2.

Fig. 9: Variations of ultrasonic velocity of the polymer melt with different barrel temperatures and screw speeds, measured with the UT6 at the barrel.

Fig. 10: Typical signals measured with the UT1 at the mold insert in Fig. 4(b) during one cycle of molding. L_{2n} (n=1,2...) is the echo reflected from the polymer/immobile mold interface, as illustrated in Fig. 5.

Fig. 11: Amplitude variations of the L^1 and L_2 echoes measured with the UT1 at the mold insert in Fig. 4(b) during one cycle of molding.

Fig. 12: Ultrasonic velocity in the polymer inside the mold cavity measured with the UT1 at the mold insert in Fig. 4(b), and variations of the amplitude of the L^1 echo in Fig. 11.

Fig. 13: Ultrasonic velocity and attenuation (a); and specific volume (b) of the POM with respect to the temperature during cooling, measured by a static ultrasonic measurement system.

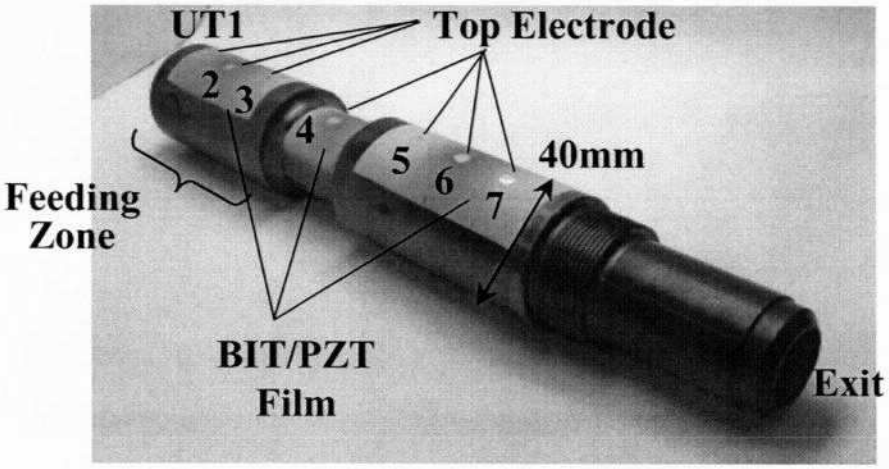
UT1
Top Electrode
2
3
4
5
6
7
40mm
Feeding
Zone
BIT/PZT
Film
Exit

Fig. 1

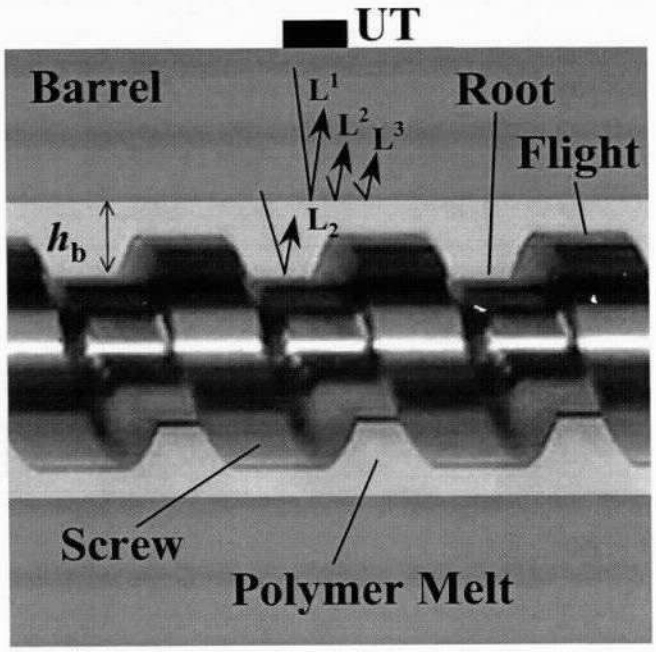

Fig. 2

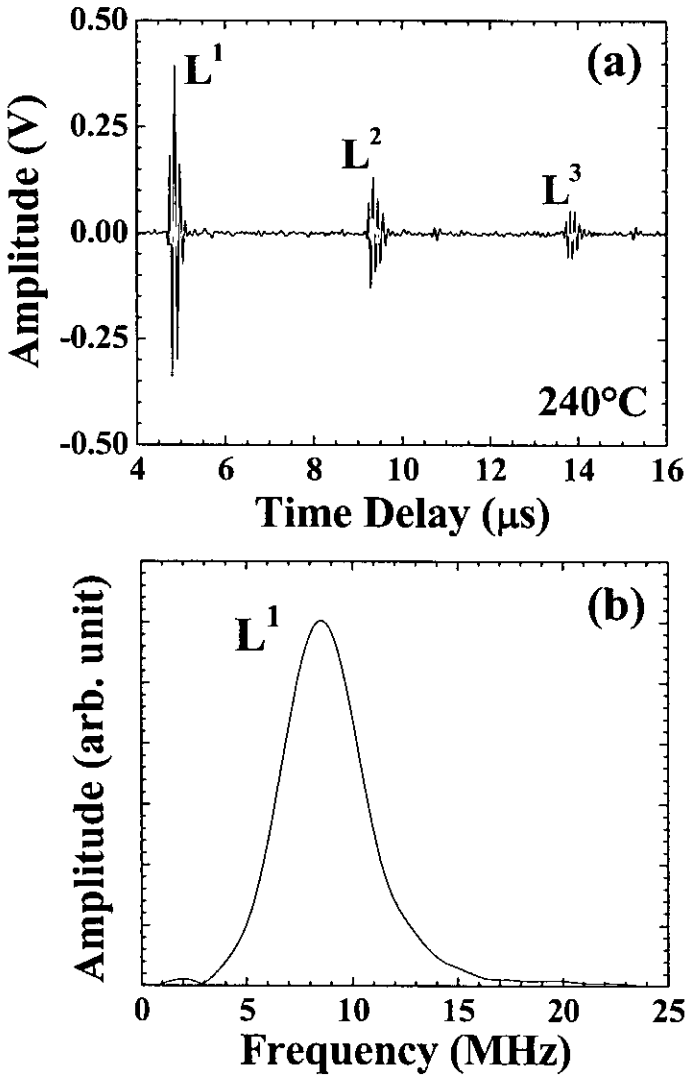
0.50
0.25
0.00
-0.25
-0.50
Amplitude (V)
L1
L2
L3
(a)
240°C
4
6
8
10
12
14
16
Time Delay (μs)
Amplitude (arb. unit)
L1
(b)
0
5
10
15
20
25
Frequency (MHz)

Fig. 3

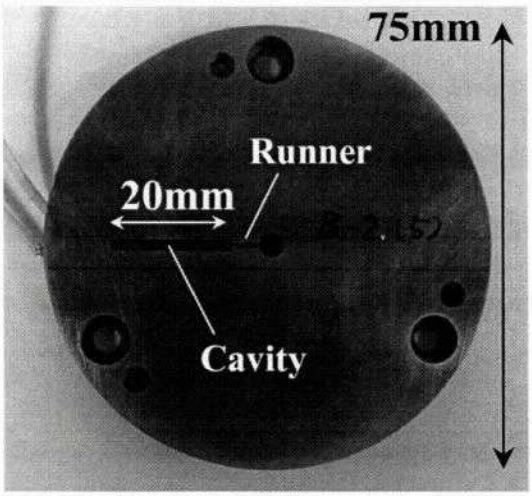

(a) Cavity (Polymer) Side

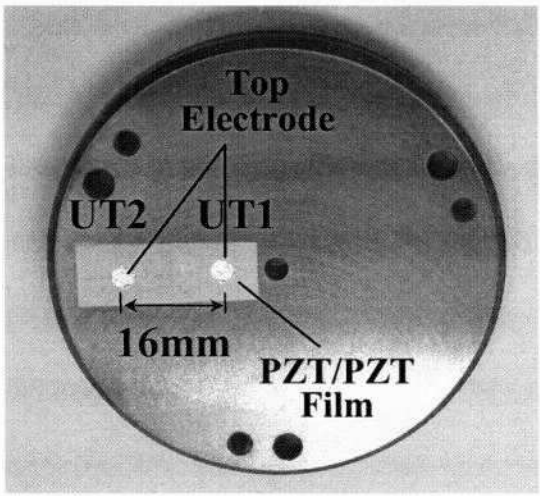

(b) UT Side

Fig. 4

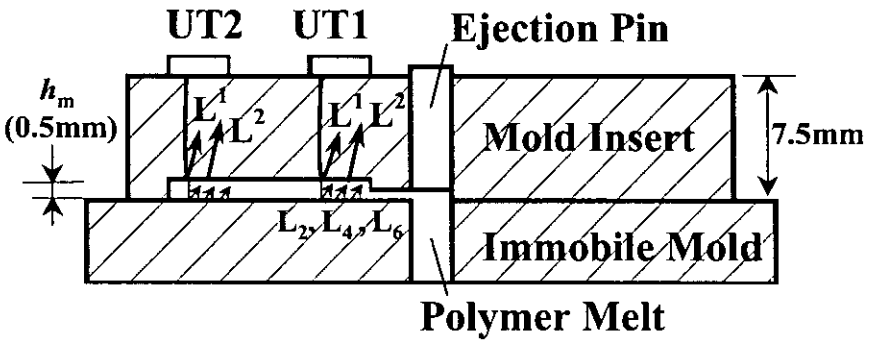
UT2
UT1
Ejection Pin
h_m
(0.5mm)
L^1
L^2
L^1
L^2
Mold Insert
7.5mm
L_2, L_4, L_6
Immobile Mold
Polymer Melt

Fig. 5

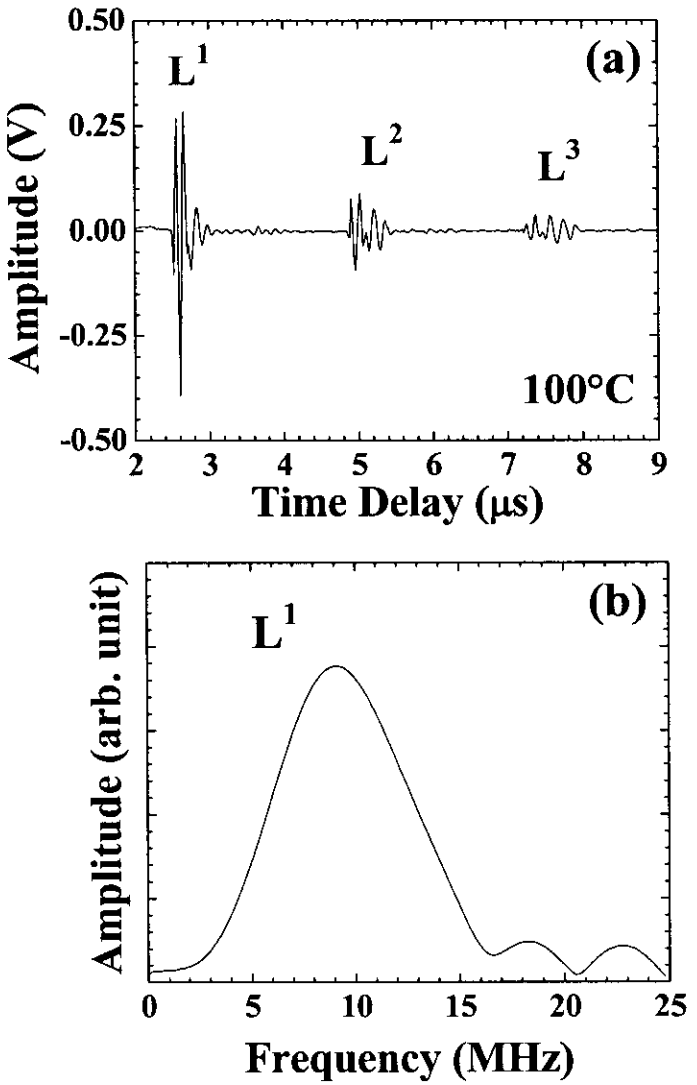
0.50
0.25
0.00
-0.25
-0.50
Amplitude (V)
L1
L2
L3
(a)
100°C
2
3
4
5
6
7
8
9
Time Delay (μs)
Amplitude (arb. unit)
L1
(b)
0
5
10
15
20
25
Frequency (MHz)

Fig. 6

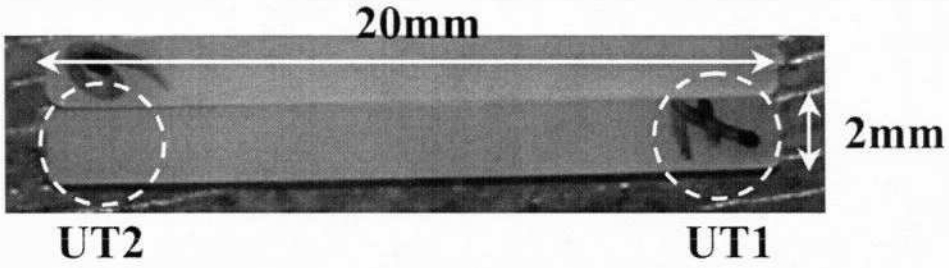

Fig. 7

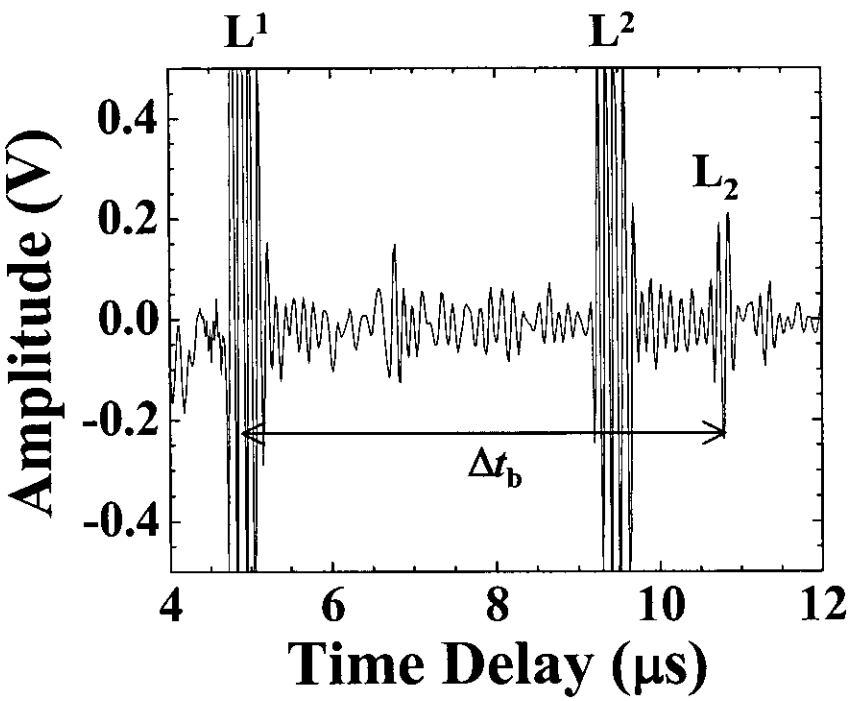

Fig. 8

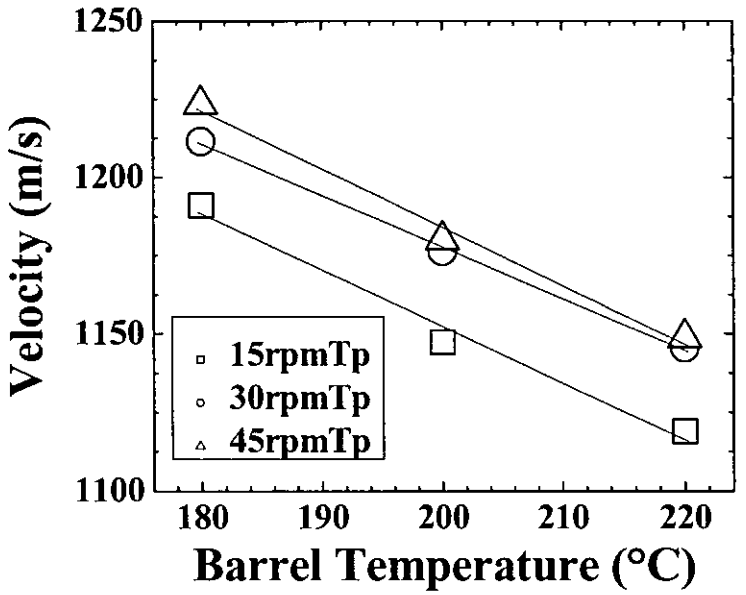
1250
1200
1150
1100
Velocity (m/s)
180
190
200
210
220
Barrel Temperature (°C)
15rpmTp
30rpmTp
45rpmTp

Fig. 9

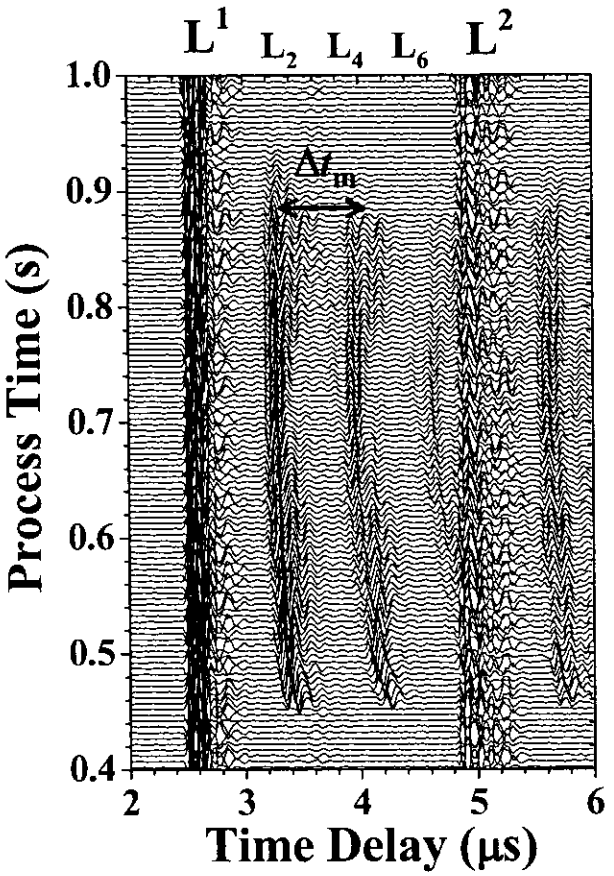
L1
L2
L4
L6
L2
Δtm
Process Time (s)
1.0
0.9
0.8
0.7
0.6
0.5
0.4
2
3
4
5
6
Time Delay (μs)

Fig. 10

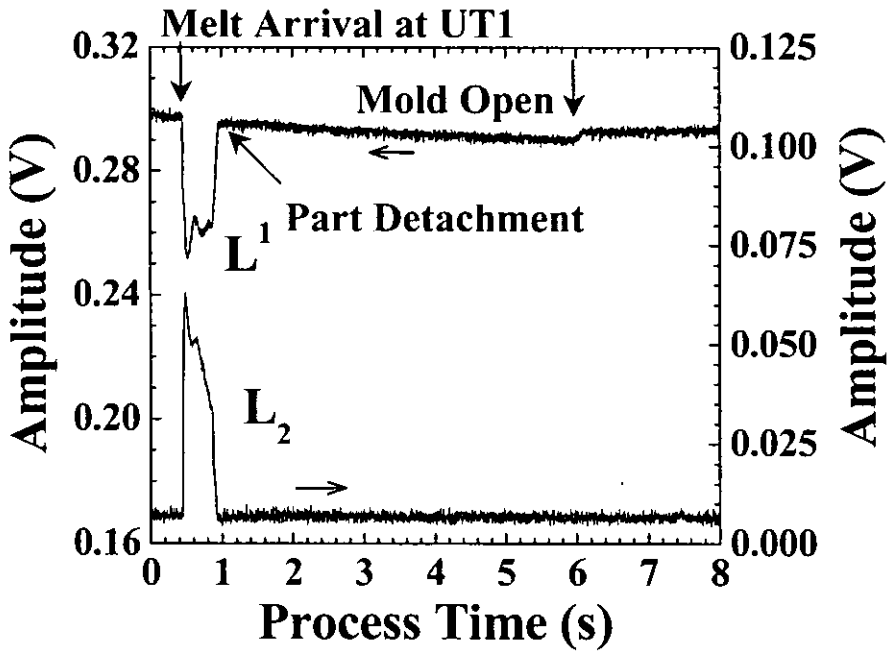
Melt Arrival at UT1
Mold Open
Part Detachment
L^1
L_2
Amplitude (V)
Amplitude (V)
Process Time (s)
0.32
0.28
0.24
0.20
0.16
0.125
0.100
0.075
0.050
0.025
0.000
0
1
2
3
4
5
6
7
8

Fig. 11

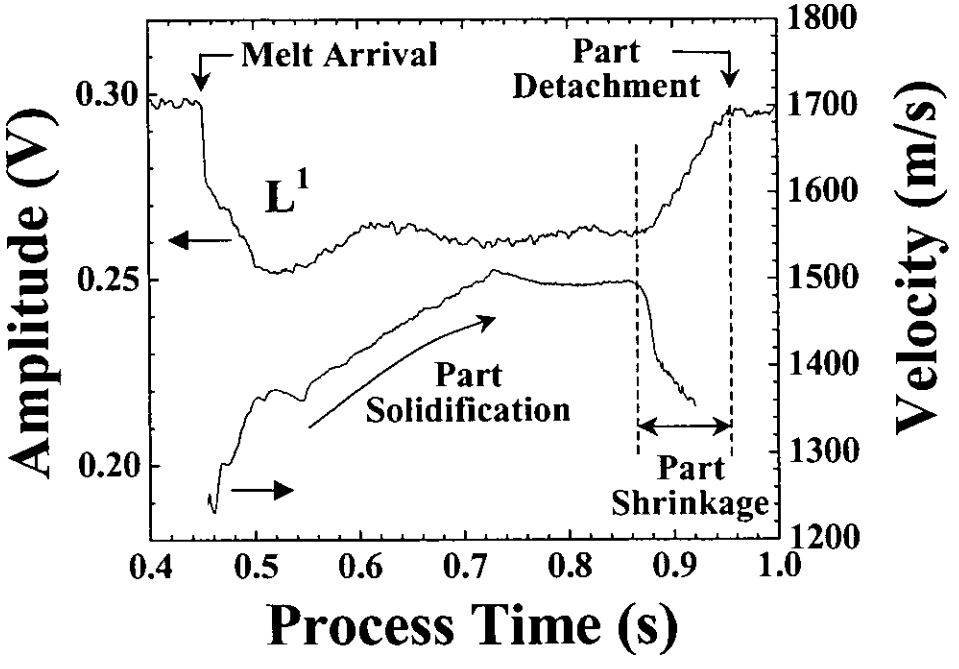
Melt Arrival
Part Detachment
L1
Part Solidification
Part Shrinkage
Amplitude (V)
Velocity (m/s)
Process Time (s)
0.30
0.25
0.20
1800
1700
1600
1500
1400
1300
1200
0.4
0.5
0.6
0.7
0.8
0.9
1.0

Fig. 12

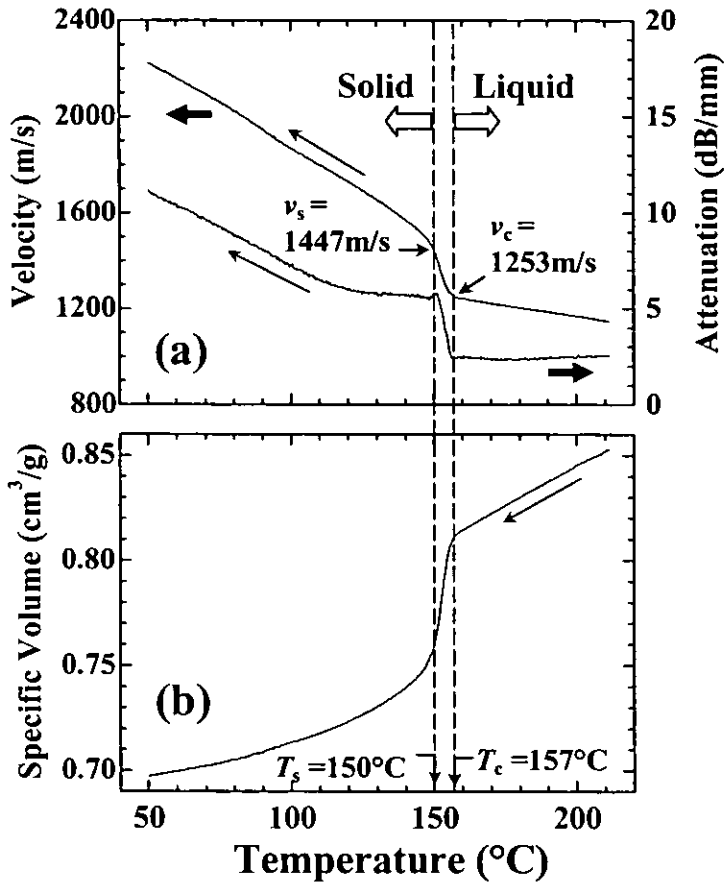
2400
2000
1600
1200
800
Velocity (m/s)
20
15
10
5
0
Attenuation (dB/mm)
Solid
Liquid
v_s =
1447m/s
v_c =
1253m/s
(a)
0.85
0.80
0.75
0.70
Specific Volume (cm^3/g)
(b)
T_s =150°C
T_c =157°C
50
100
150
200
Temperature (°C)

Fig. 13